arXiv:1607.05492v1 [physics.chem-ph] 19 Jul 2016

Concurrent parametrization against static and kinetic information leads to more robust coarse-grained force fields

Joseph F. Rudzinski and Tristan Bereau
Max Planck Institute for Polymer Research, Mainz 55128, Germany
(Dated: July 20, 2016)

The parametrization of coarse-grained (CG) simulation models for molecular systems often aims at reproducing static properties alone. The reduced molecular friction of the CG representation usually results in faster, albeit inconsistent, dynamics. In this work, we rely on Markov state models to simultaneously characterize the static and kinetic properties of two CG peptide force fields—one top-down and one bottom-up. Instead of a rigorous evolution of CG dynamics (e.g., using a generalized Langevin equation), we attempt to improve the description of kinetics by simply altering the existing CG models, which employ standard Langevin dynamics. By varying masses and relevant force-field parameters, we can improve the timescale separation of the slow kinetic processes, achieve a more consistent ratio of mean-first-passage times between metastable states, and refine the relative free-energies between these states. Importantly, we show that the incorporation of kinetic information into a structure-based parametrization improves the description of the helix-coil transition sampled by a minimal CG model. While structure-based models understabilize the helical state, kinetic constraints help identify CG models that improve the ratio of forward/backward timescales by effectively hindering the sampling of spurious conformational intermediate states.

I. INTRODUCTION

The last few decades have witnessed the onset and development of computer simulations of (macro)molecular systems, providing increasingly accurate and reliable atomic-level detail into their structure and dynamics [1–3]. For all but the smallest of systems, sufficient conformational sampling remains a significant bottleneck—notable examples include conformational transitions in proteins [3] and the insertion of small molecules in lipid membranes [4]. Concurrent to all-atom (AA) models, coarse-grained (CG) models, which reduce the number of degrees of freedom by lumping several atoms into larger beads, provide the means to probe essential aspects of these systems and push toward length- and timescales currently unattainable with AA models [5–10].

Most strategies that aim at parametrizing CG models target static properties—whether phenomenological or emergent properties in top-down models, or structural aspects of a reference higher-level simulation in bottom-up models—while kinetic information is rarely included. Thus, the resulting CG simulations display largely uncontrolled dynamics, making any kinetic-based conclusion difficult to interpret. More specifically, CG dynamics commonly exert *faster* behavior compared to AA simulations or experiments, which can be rationalized by the model's reduced molecular friction [11]. While faster dynamics works to the simulator's advantage—providing more efficient conformational sampling and transitions—meaningful dynamical information about the system can only be extracted if *all* kinetic processes are sped up uniformly or in a predictable fashion. While rescaling CG dynamics by a single speed-up factor has proven useful for individual kinetic observables, e.g., collapse of the mean-squared displacement of various polymer melts across chain lengths [12, 13], correcting a variety of coupled kinetic processes remains problematic.

More rigorous approaches to describing accurate dynamics in CG models require additional parametrization effort. The Mori-Zwanzig formalism describes the dynamical evolution of a CG system by means of a generalized Langevin equation, in which the noise and friction need careful attention to accurately model local dynamics [14, 15]. Practically, this entails the parametrization of a friction *tensor* for each CG bead [16–20]. Other efforts have focused on emulating friction tensors via fictitious particles [21], the estimation of entropy and friction corrections due to coarse-graining [22], or choosing the CG mapping to minimize memory [23]. Clearly, while the static properties of a simulation model only depend on its force field, its kinetics depend additionally on the applied thermostat—making the latter's choice and parametrization essential.

Building upon these efforts, we seek a simple and systematic method capable of both analyzing and improving kinetic properties in CG models. Specifically, we take two main considerations into account:

1. Many molecular systems display a variety of kinetic processes at various timescales. Identifying a representative set of kinetic processes and selecting relevant observables to probe them requires significant insight into the system. Ideally, manual selection of kinetic observables and processes should be avoided.

2. Rigorous approaches to building consistent dynamics in CG models have three main disadvantages: (*i*) They are often tedious to parametrize and implement (e.g., optimization and numerical integration of friction tensors); (*ii*) They scale *down* the accelerated dynamics of CG models to the level of the real system—reducing the sampling efficiency closer to AA models. From a practical perspective, CG models should ideally exhibit both faster

and *consistent* dynamics; and lastly (*iii*) The long-timescale effects from assumptions and errors associated with the local kinetic parameters (e.g., friction tensor) can be difficult to control.

Markov state models (MSMs) [24–26], which are coarse-grained kinetic models of a simulation trajectory, specifically address the first point. In particular, by estimating transition probabilities between predefined microstates, a diagonalization of the resulting transition probability matrix provides an immediate characterization of the hierarchy of slowest timescales (i.e., eigenvalues) and associated processes (i.e., eigenvectors). For systems at equilibrium, the largest eigenvalue (i.e., $\lambda_0 = 1$) corresponds to an infinite timescale with an associated eigenvector describing the stationary distribution projected onto the chosen microstates. Consequently, MSMs simultaneously characterize the static and kinetic properties of the system, making them a useful methodology to analyze simulation models [27–33].

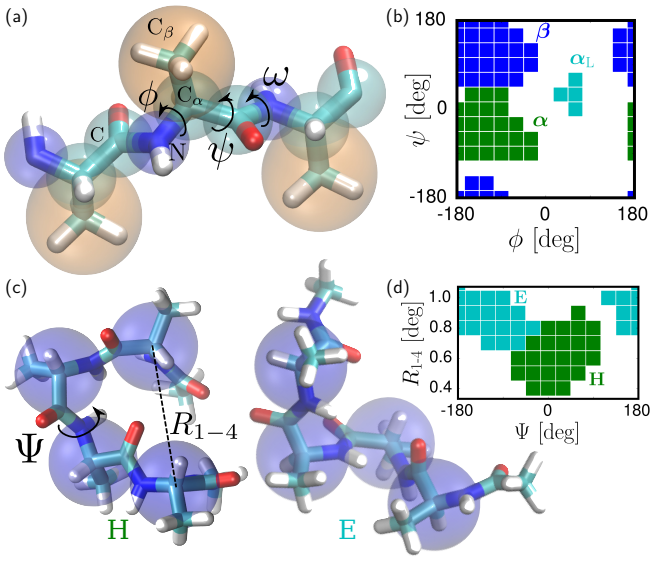

FIG. 1. (a) Cartoon representation of an Ala_3 peptide. Atoms are shown using a licorice representation (without terminals), while CG beads of the PLUM model are displayed as spheres. The different beads consist of: N for the amide group, C_α for the central carbon, C_β for the side chain, and C for the carbonyl group. The backbone dihedrals ϕ, ψ, and ω are depicted as well. (b) Illustration of the three relevant metastable states for Ala_3 sampled by PLUM, projected on a Ramachandran map: helical (α), extended (β), and left-handed helix (α_L) regions. (c) Cartoon representation of an Ala_4 peptide. Representations of the helical (H) and extended (E) metastable states are shown, as well as the dihedral, Ψ, and 1–4 residue distance, R_{1-4}, order parameters. (d) Illustration of the two relevant metastable states for Ala_4 sampled by CG-sb, projected onto the two order parameters. Cartoons rendered with VMD [34].

We recently reported the use of MSMs to analyze two CG peptide models—one top-down and one bottom-up (Figure 1) [35]. Peptides offer a useful test for CG models as they display a variety of kinetic processes at overlapping timescales—even for the smallest of systems. We probed to what extent the simulation trajectories were compatible with more consistent kinetics by building *biased* MSMs, which attempt to balance the microstate transitions observed in CG simulation trajectories and reference kinetic information by reweighting the transition probability matrix. In this work, we propose refinements to the two peptide models by altering their force field based on this reweighting. By focusing on improving not only the stationary distribution but also ratios of timescales (i.e., up to an arbitrary speed-up factor) and a qualitative description of the associated eigenvectors, we use the MSM framework to refine both the static and kinetic properties of the CG models. Rather than reference AA simulations, the present reparametrization relies on biased MSMs for two reasons: (*i*) this strategy is helpful when no AA simulations are available (e.g., but only CG simulations and experimental information) and (*ii*) biased MSMs can help guide *how* to reparametrize the CG model. To keep the parametrization and implementation procedure simple, we limit changes to the CG models to the beads' masses (i.e., effectively scaling individual isotropic friction coefficients) and a small number of relevant force-field parameters. Though these adjustments are not enough to recover a rigorous dynamical evolution of the systems, we show that they help enhance the quality of the CG models—not only kinetic, but also static properties.

The present work demonstrates that relying on a combination of static and kinetic information can help construct more robust CG force fields. We find that a simple rescaling of the masses can shift the relative timescales of the slow kinetic processes, without affecting their nature (i.e., corresponding eigenvector) or ratio of forward/backward timescales. As a result, mass rescaling does not necessarily help correct the ordering of the processes. Larger alterations of the kinetics require force-field adjustments. For example, we consider the helix-coil transition sampled by a minimal CG model for a small peptide. It was previously demonstrated that a structure-based parametrization—aimed at reproducing low-order correlation functions—understabilized the helical state and sampled a large basin of spurious conformational intermediate states [36]. We demonstrate here that the inclusion of kinetic constraints into the parametrization procedure helps identify an alternative CG model that retains the essential static properties of the original CG model, while improving the ratio of forward/backward timescales by effectively hindering the sampling of these spurious intermediates.

II. MODELS AND METHODOLOGY

In this work, we investigate the impact of incorporating kinetic information into the parametrization of CG mod-

els. We consider two small peptide systems along with two distinct CG approaches: (*i*) a transferable model that retains resolution of the peptide backbone dihedrals and (*ii*) a highly-specific, structure-based, 1-bead per amino acid model. For reference, we use explicitly solvated AA simulations of the corresponding capped peptides, which employ the OPLS-AA [37] and SPC/E [38] force fields to model the peptide and solvent interactions, respectively. These simulations consisted of a total of 1 μs from five independent simulations and were described previously [35, 36].

A. Transferable CG PLUM model applied to Ala_3

a. Model PLUM describes an amino acid using four beads—three for the backbone and one for the side chain—in an implicit water environment [39]. The almost-atomistic resolution of the backbone allows an explicit modeling of the backbone dihedrals, ϕ, ψ, and ω (Figure 1). While ω—centered around the peptide bond—is largely frozen, ϕ and ψ display significant variability and directly map to larger-scale peptide secondary structures. As such, ϕ and ψ are commonly employed in Ramachandran maps [40] to analyze the conformational variability of small peptides.

PLUM was parametrized using a top-down strategy [10], which consists of incorporating interactions that are deemed relevant, and whose parameters are optimized to reproduce emerging properties of the system. In PLUM, the parametrization of local interactions (e.g., sterics) aimed at a qualitative description of Ramachandran maps, while longer-range interactions—hydrogen bond and hydrophobicitiy—aimed at reproducing the folding of a three-helix bundle, without explicit bias toward the native structure [39]. The model is generic in that it aims at describing the essential features of a variety of amino-acid sequences, rather than an accurate reproduction of any specific one. After parametrization, it was shown capable to fold several helical peptides [39, 41–44], stabilize β-sheet structures [39, 45–48], and used to probe the conformational variability of intrinsically disordered proteins [49].

The kinetics of the PLUM peptide model were probed by means of a Markov state model analysis of a tripeptide of alanine residues (Ala_3) [35]. Compared with reference AA simulations, the results pointed at significant issues with the reproduction of the relative timescales of the slowest processes. Worse, the CG model switches the order of the two slowest processes: the transition in and out of the left-handed helical region, α_{L}, and the $\alpha - \beta$ transitions (see Figure 1 (b) for a projection of these metastable states on the Ramachandran map). The incorporation of reference mean-first-passage times between the α, β, and α_{L} regions of the Ramachandran map led to a biased Markov state model that captured the essential features of the CG simulations, while yielding a realistic hierarchy of kinetic processes and correct timescale separation [35].

b. Simulations CG simulations of Ala_3 with the PLUM force field [39, 50, 51] were run using the ESPResSo simulation package [52]. Details of the force field, implementation, and simulation parameters can be found in Bereau and Deserno [39]. CG units of the model are built from a length, $\mathcal{L}^{\mathrm{P}} = 1$ Å, an energy $\mathcal{E}^{\mathrm{P}} = k_{\mathrm{B}}T_{\mathrm{room}} \approx 0.6$ kcal/mol as the thermal energy at room temperature, and a mass $\mathcal{M}^{\mathrm{P}} \approx 4.6 \times 10^{-26}$ kg [39]. The CG unit of time can be constructed from the combination $\mathcal{T} = \mathcal{L}\sqrt{\mathcal{M}/\mathcal{E}}$. Using the values above, we find $\mathcal{T}^{\mathrm{P}} \sim 0.1$ ps, which does *not* realistically represent the conformational changes of the protein [35, 39]. A single canonical simulation at temperature $k_{\mathrm{B}}T = 1.0\ \mathcal{E}$ was performed for $100,000\ \mathcal{T}^{\mathrm{P}}$, recording the system every $0.1\ \mathcal{T}^{\mathrm{P}}$. Temperature control was ensured by means of a Langevin thermostat with friction coefficient $\gamma = (1.0\ \mathcal{T}^{\mathrm{P}})^{-1}$.

c. Reparametrization For the purpose of the present reparametrization, we first varied the masses, m, of the beads. While all set to $m = \mathcal{M}$ in the original model [39], we considered alternative assignments for the C_α, C_β, and C beads, while retaining $m_{\mathrm{N}} = \mathcal{M}$ (Figure 1). Fixing the mass of one of the beads allows us to focus on altering the *relative* kinetics, since a uniform shift of all masses merely scales each dynamical process by the same amount. We considered alternative masses $m/\mathcal{M} = \{0.1, 0.5, 1.0, 2.0, 5.0, 10.0\}$, for a total of $6^3 = 216$ trial models.

The PLUM force field is made up of a small number of interactions. Excluding the bonded interactions, there are steric interactions between beads, the backbone-backbone hydrogen-bond interaction, and side-chain hydrophobicity. The last two have little effect on the static and kinetic properties of Ala_3, given the small size of the system. Thus, we focus on the sterics, varying the Weeks-Chandler-Anderson parameters associated with the bead sizes, σ, within 10% of their original values (the functional form makes the interactions insensitive to the strength, ϵ). For each reparametrization, we ran a canonical simulation and analyzed both the static and kinetic properties using a Markov state model analysis.

B. Structure-based CG model for Ala_4

d. Model We also considered a system-specific, structure-based implicit solvent CG model [36] for a tetra-peptide of alanine residues (Ala_4), effectively probing a minimal helix-coil transition. This model, denoted CG-sb, represents each amino acid with a single CG bead, placed at the α-carbon position. The potential energy function employs four distinct interactions between the four CG beads: bond, angle, dihedral and 1–4 (i.e., end-to-end). These potentials were determined using a self-consistent generalized Yvon-Born-Green relation [53, 54] aimed at reproducing a set of force correlation functions—related to one-dimensional structural

distributions—along each order parameter corresponding to a term in the CG potential. The CG-sb model qualitatively reproduces the free-energy surface along the dihedral angle, Ψ, defined between the four α-carbons of the peptide backbone and the end-to-end distance, $R_{1\text{–}4}$, between the first and last α-carbons (Figure 1c). Although CG-sb better stabilizes helices compared to a corresponding force-matching-based model, the minimal representation and simple interactions lead both models to sample a large basin of spurious conformational intermediates, forbidden at the AA level [36].

The kinetics of the CG-sb model were also recently assessed via Markov state model analysis [35]. Compared to reference AA simulations, the CG-sb model correctly assigns the transition between helical (H) and extended (E) metastable states as the slowest dynamical process, and with an accurate representation of the associated eigenvector (i.e., which microstates are primarily involved in the kinetic process). However, the CG-sb model exhibits transitions from H to E that are too fast compared to the backward process, in line with the understabilized helical state [36]. The model also lacks any significant timescale separation between the two slowest dynamical processes [35]. The incorporation of reference mean-first-passage times between the H and E metastable states led to a biased Markov state model that retained the essential features of the original model, while improving the timescale separation and the ratio of forward/backward timescales of the H−E transition. This improvement was achieved by concentrating the flux of probabilities in a narrow subset of the helical region, as compared to the reference AA trajectory.

e. Simulations CG simulations of Ala_4 were performed with the Gromacs 4.5.3 simulation suite in the constant NVT ensemble with $T = 298$ K, while employing the stochastic dynamics algorithm with a friction coefficient $\gamma = (2.0\ \mathcal{T}^{\mathrm{S}})^{-1}$ and a time step of $1e-3\ \mathcal{T}^{\mathrm{S}}$, where $\mathcal{T}^{\mathrm{S}} = 1$ ps. A single simulation was performed for $50,000\ \mathcal{T}^{\mathrm{S}}$, recording the system every $0.05\ \mathcal{T}^{\mathrm{S}}$. The CG unit of time, $\mathcal{T}^{\mathrm{S}}$, can be determined from estimates of the fundamental units of length, mass, and energy of the simulation model, but does not provide any meaningful description of the dynamical processes generated by the model.

f. Reparametrization We considered several reparametrizations of the CG-sb model, which employ the same representation and set of interaction types as the original model. The bond potential remained identical for all models. Our reparametrization strategy follows the insight gained from the biased Markov state model: vary parts of the CG potentials to better stabilize the helical state [35]. As a proxy, we take the difference between the CG-sb and force-matching potentials, δU_i, given the models' differing abilities in stabilizing the helix [36]. Trial CG potentials were then defined as $U_i^{\mathrm{CG}}(\boldsymbol{\alpha}) = U_i^{\text{CG-sb}} + \alpha_i \delta U_i$, where $i = \{\text{ang, dih, 1–4}\}$ adjusts separately each angle, dihedral, and 1–4 interaction, respectively. For each reparametrization, we ran a canonical simulation and analyzed both the static and kinetic properties using a Markov state model analysis.

C. Markov state models

Given a trajectory generated from molecular dynamics simulations, Markov state models attempt to approximate the exact dynamical propagator with a finite transition probability matrix, $\mathbf{T}(\tau)$ [24–26]. This requires a discretization of configuration space, which groups all possible configurations into a manageable set of microstates. Once the microstates are chosen, the number of observed transitions from microstate i to j at a time separation τ, $C_{ij}^{\mathrm{obs}}(\tau)$, is determined. The matrix of transition counts, $\mathbf{C}^{\mathrm{obs}}(\tau)$, embodies the dynamics of the simulation trajectory. An estimator for the transition probability matrix is then constructed such that the simulation data is optimally described, while ensuring normalization and detailed balance constraints. The latter constraint applies to any system at equilibrium and alleviates finite-sampling issues. The transition probability matrix is constructed by maximizing the posterior $p(\mathbf{T} \mid \mathbf{C}) \propto p(\mathbf{C} \mid \mathbf{T}) = \prod_{i,j} T_{ij}^{C_{ij}}$, where we applied Bayes' theorem and a uniform prior distribution [55].

We recently proposed a method to construct an MSM informed by additional external information [35]. By combining the aforementioned optimization procedure with a set of *coarse* reference kinetic constraints, we determined a new transition probability matrix that best reproduces the constraints while minimally biasing the simulation data. We refer to such models as biased MSMs.

In the present work, standard MSMs are built for each of the reparameterized CG models, as well as the reference AA models. Following the projection and discretization of peptide trajectories along the order parameters presented in Figure 1, MSMs were generated via a maximum-likelihood technique [56]. MSM construction and analysis (e.g., calculation of the eigenspectrum, metastable states, and mean-first-passage times) were performed using the pyEmma package [57–59]. Lag times of $\tau = 250$ ps and $\tau = 1.25\ \mathcal{T}^{\mathrm{S}}$ were employed for the AA and CG models, respectively, for Ala_4 and $\tau = 40$ ps and $\tau = 1.5\ \mathcal{T}^{\mathrm{P}}$ were employed for the AA and CG models, respectively, for Ala_3.[1] See the Supporting Information section of [35] for more details.

D. Model assessment

For all reparametrizations considered, we systematically compared the results to the biased Markov state

[1] Rudzinski *et al.* [35] mistakenly reported AA lag times in ns instead of ps.

models constructed by Rudzinski *et al.* [35]. We quantify the similarity between eigenvectors or stationary distributions of different models using the Jensen-Shannon divergence

$$\mathrm{JSD}(p||q) = \frac{1}{2}\sum_i p_i \left(\ln p_i - \ln m_i\right) + \frac{1}{2}\sum_j q_j \left(\ln q_j - \ln m_j\right), \tag{1}$$

where p and q are two (discretized) distributions, i and j run over all bins, and $m = (p+q)/2$. The JSD provides a symmetrized and smoothed version of the Kullback-Leibler divergence, $D(p||q) = \sum_i p_i \ln p_i/q_i$ [60].

III. RESULTS

A. Transferable PLUM model applied to Ala_3

The following describes the refinement of the PLUM model to better describe the statics and kinetics of Ala_3. As a first step, we monitor to what extent varying the beads' masses can help improve the kinetic properties of the model. Given that masses only couple to the Hamiltonian via the kinetic energy, they do not alter any static equilibrium property [61]. Thus, we only monitor the impact on the dominant eigenvalues and eigenvectors of the transition probability matrix. Subsequently, we consider larger changes to PLUM by varying force-field components and assess both static and kinetic properties of the resulting models.

We begin with a brief summary of the kinetic analysis of PLUM applied to Ala_3, reported by Rudzinski *et al.* [35]. Reference AA simulations indicated a strong timescale separation between the second eigenvalue and the next—singling out the first two kinetic processes as the most relevant. These correspond to transitions *between* the metastable states depicted in Figure 1 (b)—in and out of α_L and between α and β, respectively—while all other kinetic processes occur *within* the metastable states. Although the AA MSM yielded very similar eigenvalues, $\lambda_2/\lambda_1 \approx 0.9$, the PLUM MSM displayed a first eigenvalue that is too high compared to the second, i.e., $\lambda_2/\lambda_1 \approx 0.4$ (Figure 2). Worse, the order of the first two eigenvectors in PLUM is switched, such that the ratio between λ_1 and λ_2 is qualitatively wrong.

g. Refinement I: masses To probe the dependence of the kinetic properties of PLUM's Ala_3 on the masses, we considered a variety of bead-mass combinations as described in the Methods section. Importantly, all models keep $m_N = \mathcal{M}$ fixed, such that the effect stems from the *difference* between masses. For each model, we monitor the accuracy of the *relative* timescales of the first two kinetic processes, λ_2/λ_1, as shown in Figure 3 (a).

Among all beads, we find the strongest variations against m_C. Increasing m_C/m_N is expected to slow processes along ϕ, since this dihedral directly connects the C beads of consecutive residues. Kinetically, motion along ϕ correlates most strongly with transitions between the α_L and β regions (Figure 1). Indeed, we find that increasing m_C/m_N slows down the second kinetic process in PLUM (i.e., transitions involving α_L) with respect to the first (i.e., $\alpha - \beta$ transitions), such that λ_2/λ_1 improves (Figure 3 (a)). However, even a ratio m_C/m_N approaching 10^2—arguably an unreasonably large difference—does not suffice to reach $\lambda_2 = \lambda_1$, at which point the two eigenvalues switch to correct the order of the kinetic processes.

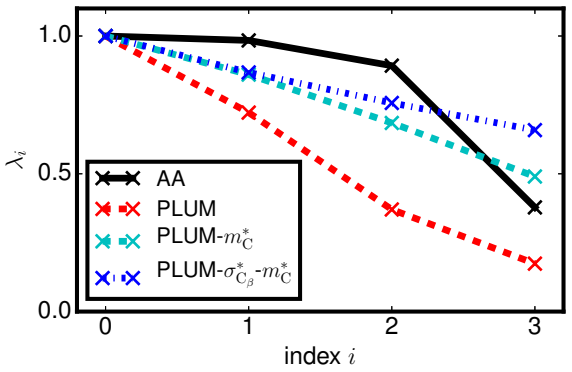

FIG. 2. Ala_3: Eigenvalue spectrum of the three slowest processes of the reference AA model, the original PLUM model, PLUM with rescaled masses (PLUM-m_C^*), and PLUM with altered force field and rescaled masses (PLUM-$\sigma_{C_\beta}^*$-m_C^*). Starting with λ_3, the corresponding kinetic processes probe transitions *within* metastable states.

To further probe the ordering of kinetic processes, Figure 3 (b) reports the Jensen-Shannon divergence (JSD; equation 1) between eigenvectors of identical index, as well as between eigenvectors of different indices. Overall, the trial simulation models with altered masses yielded similar eigenvectors and none of them corrected the hierarchy of kinetic processes. The eigenvalue spectrum of an improved mass-rescaling is presented in Figure 2 (PLUM-m_C^*), for which $m_C = 10\,\mathcal{M}$ while $m_{C_\alpha} = m_N = \mathcal{M}$. The eigenvalue ratio of PLUM-m_C^*, $\lambda_2/\lambda_1 = 0.8$, is significantly improved compared to the original PLUM model. However, mass rescaling does not significantly change the ratio of forward/backward mean-first-passage times between pairs of metastable states (data not shown). Altering masses likely scales the dynamics homogeneously across a particular kinetic process, whether forward or backward.

All in all, these findings suggest that mass rescaling can improve the relative timescale of different kinetic processes, but cannot improve relative mean-first-passage times, and is not necessarily sufficient to correct qualitative discrepancies in the model's kinetic properties.

h. Refinement II: force field Though we attempted to vary all bead sizes around their equilibrium values, the side chain yielded the largest effects on both the static and kinetic properties. Specifically, reducing the side-chain bead radius, σ_{C_β}, by 10% (i.e., from 2.50 Å to

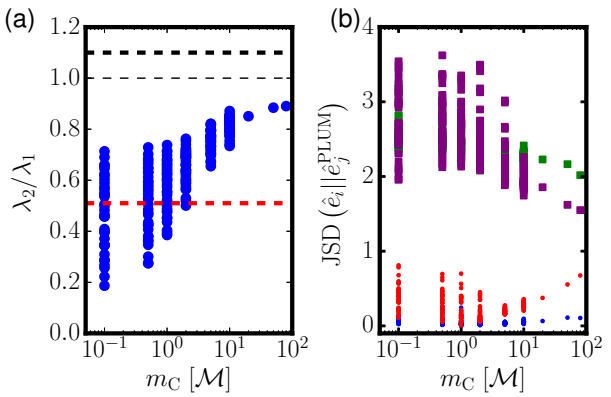

FIG. 3. Ala_3: (a) Ratio of the first two eigenvalues λ_2/λ_1, indicating the relative timescale of the associated kinetic processes. The bold red and black dashed lines indicate values for the original PLUM and reference AA models, respectively. Note that the AA ratio is located above 1.0 because of PLUM's unphysical switching of the kinetic processes. Blue dots correspond to trial CG models with rescaled masses, projected along m_{C} while $m_{\mathrm{N}} = \mathcal{M}$. (b) Jensen-Shannon divergence (equation 1) between eigenvectors of the trial models and the original PLUM model: red and blue dots are between eigenvectors of identical index (i.e., $1-1$, $2-2$), while the purple and green squares are between eigenvectors of different indices (i.e., $1-2$, $2-1$).

2.25 Å) significantly altered several properties of the force field. Figure 4 (a–c) compares the free-energy surfaces of the AA, PLUM, and the altered PLUM force field with reduced side-chain bead size (PLUM-$\sigma^*_{\mathrm{C}_\beta}$). We find a significant stabilization of the sterically-hindered region with $\phi \approx 120$ deg and $\psi \approx -120$ deg. Though too stable compared to the AA model, the free-energy of this region remains in the range $\approx 2{-}6\ k_{\mathrm{B}}T$, such that the conformational ensemble at room/body temperature is marginally affected. Further, this leads to an improved description of the α_{L} metastable state: the free-energy of α_{L} relative to β was previously reported as 4.18 and 5.75 $k_{\mathrm{B}}T$ for the AA and original PLUM models [35], while PLUM-$\sigma^*_{\mathrm{C}_\beta}$ yields 4.10 $k_{\mathrm{B}}T$, in excellent agreement with AA. Similarly, the free-energy of α relative to β is improved: values of 0.42, 0.95, and 0.65 $k_{\mathrm{B}}T$ are found for the AA, PLUM, and PLUM-$\sigma^*_{\mathrm{C}_\beta}$ force fields, respectively. Figure 4 (d–f) also displays projections of the AA metastable states, sampled in the CG trajectories. We find that the PLUM-$\sigma^*_{\mathrm{C}_\beta}$ model displays a broader α_{L} region as compared to PLUM, in better agreement with AA. Kinetic properties are improved slightly, as evidenced by a larger eigenvalue ratio, $\lambda_2/\lambda_1 = 0.75$, though we obtain eigenvectors similar to PLUM's.

Evidently, the altered force field should not only improve the description of the Ramachandran map, it ought to retain the features of the original model. Given that PLUM was parametrized to also reproduce the folding of the *de novo* α3D three-helix bundle, we verified that PLUM-$\sigma^*_{\mathrm{C}_\beta}$ could do the same using the original simulation protocol [39]. We indeed find spontaneous folding, as monitored by the amount of helicity and topology of the three helices against the NMR structure [62], and a virtually unaltered folding temperature, i.e., $k_{\mathrm{B}}T_f \approx 1.2\ \mathcal{E}$ (data not shown).

Finally, applying the mass rescaling proposed above, we obtain a model (PLUM-$\sigma^*_{\mathrm{C}_\beta}$-$m^*_{\mathrm{C}}$) that further increases the eigenvalue ratio, $\lambda_2/\lambda_1 = 0.87$, only 20% off from the AA ratio, while the original PLUM model was more than 50% too low (Figure 2). In terms of mean-first-passage times, PLUM-$\sigma^*_{\mathrm{C}_\beta}$-$m^*_{\mathrm{C}}$ slightly improves the forward/backward timescale ratio for transitions between the metastable states (data not shown).

B. Structure-based model for Ala_4

We also assessed refinements of the CG-sb model to better reproduce features of the helix-coil transition for Ala_4. We consider variations in the angle, dihedral, and 1–4 potentials of the CG-sb model according to individual scaling parameters, α_i, for each interaction i. Figure 5 illustrates characteristics of the resulting interaction potentials for the dihedral and 1–4 degrees of freedom. Panel (a) demonstrates that the minima in the dihedral interaction corresponding to the helix (H, $\Psi \approx 60$ deg) and extended (E, $\Psi \approx -120$ deg) regions become increasingly narrow as α_{dih} shifts from -1 (red curve) to 2.5 (blue curve). The E minimum also shifts significantly to the right—a limitation of our parameter search. In addition to the narrowing, the H region is stabilized relative to E. Similarly, panel (b) demonstrates that the H minimum ($R_{1\text{–}4} \approx 0.5$ nm) in the 1–4 interaction is both narrowed and destabilized as $\alpha_{1\text{–}4}$ shifts from -0.25 (red curve) to 1.25 (blue curve). The black curve in each panel of Figure 5 denotes the interaction in the CG-sb model. Finally, adjustments of the angle parameter ($0 < \alpha_{\mathrm{ang}} < 1.5$) tilted the potential to stabilize the H region relative to E.

When considering trial reparametrizations, we monitor both the reproduction of the kinetic properties against the biased MSM [35] and structural properties compared to the original parametrization [36]. In particular, improvements in the kinetics were assessed from the Jensen-Shannon divergence (JSD; equation 1) of the first dynamical eigenvector, $\hat{\boldsymbol{e}}_1$, with respect to the biased MSM, while divergence from the structural properties of the CG-sb model was quantified with the JSD of the stationary distribution, $\boldsymbol{\pi}$.

Columns 1 through 4 of Figure 6 characterize these two metrics for increasing values of the angle reparametrization parameter, α_{ang}, as a function of α_{dih} and $\alpha_{1\text{–}4}$ (see Figure 5). Figure 6 (a) demonstrates that the CG-sb model ($\boldsymbol{\alpha} = \{0, 0, 0\}$) lies away from any local minimum of JSD($\hat{\boldsymbol{e}}_1$ || $\hat{\boldsymbol{e}}_1^{\mathrm{BMSM}}$). Increased values of $\boldsymbol{\alpha}$ tend to improve the kinetics relative to the CG-sb model. Figure 6

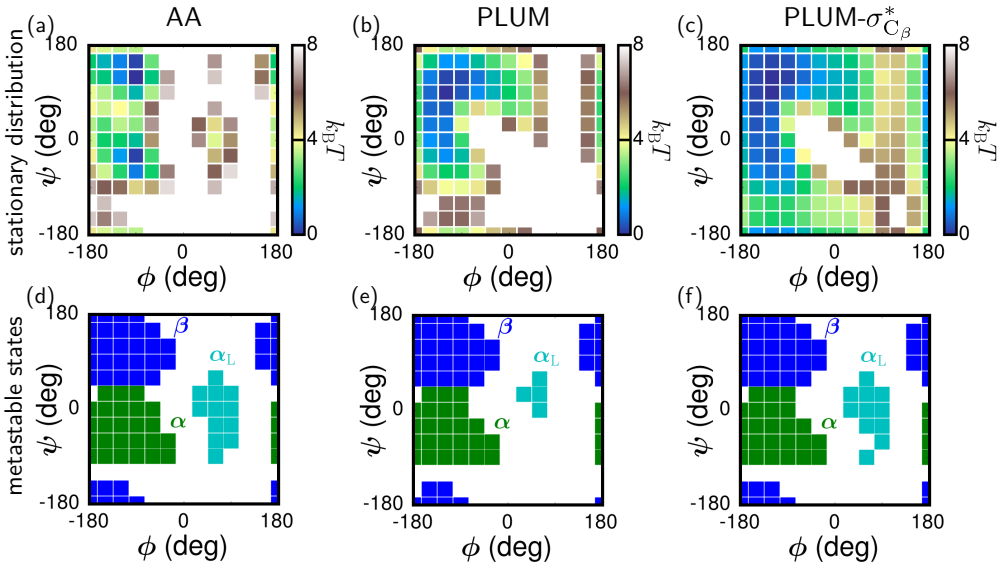

FIG. 4. Ala_3: Free-energy surfaces of AA (a), original PLUM (b), and PLUM with smaller side-chain radius, PLUM-$\sigma^*_{C_\beta}$ (c). PLUM-$\sigma^*_{C_\beta}$ almost quantitatively reproduces the $\alpha - \beta$ as well as $\alpha_L - \beta$ free-energy differences, with respect to the AA model. Metastable states of the AA model (d) and the corresponding states sampled in the two CG models: (e) PLUM and (f) PLUM-$\sigma^*_{C_\beta}$.

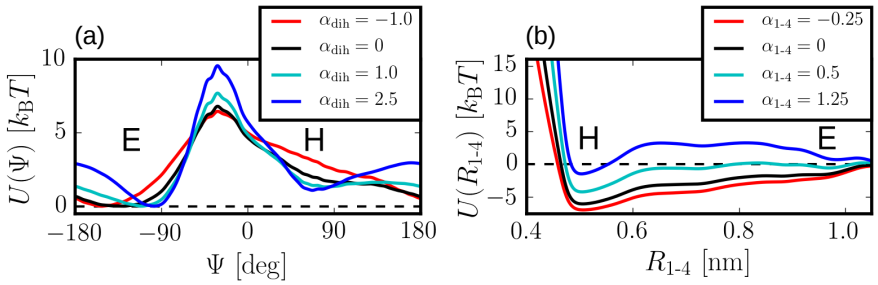

FIG. 5. Ala_4: Reparametrizations of the dihedral (a) and 1–4 (b) potentials for the CG-sb model of Ala_4 as a function of the parameter $\boldsymbol{\alpha} = \{\alpha_{ang}, \alpha_{dih}, \alpha_{1\text{–}4}\}$. The black curves correspond to the CG-sb model ($\boldsymbol{\alpha} = \{0, 0, 0\}$), while the cyan curves correspond to the reparametrized CG* model ($\boldsymbol{\alpha} = \{1.0, 1.0, 0.5\}$). The H and E labels refer to the helical and extended metastable states, respectively (see Figure 1 (d)).

(b) demonstrates that, while changing $\boldsymbol{\alpha}$ necessarily increases JSD($\boldsymbol{\pi}$ || $\boldsymbol{\pi}^{\text{CG-sb}}$), there exists a slow direction of divergence (i.e., approximately along $\delta\boldsymbol{\alpha} = \{c, c, c/2\}$, for $c > 0$). Using these metrics, we identify a set of parameters that yields a compromise between kinetics and statics. We select $\boldsymbol{\alpha} = \{1.0, 1.0, 0.5\}$ (denoted CG*) for further analysis below.

In the following, we analyze the structural and kinetic properties of the CG* model with respect to the CG-sb and reference AA models. Figure 7 (a) presents the free-energy surface of each model along Ψ and $R_{1\text{–}4}$. CG* demonstrates a stabilized H region, $p(\text{H}) = 0.39$, compared with the CG-sb model, $p(\text{H}) = 0.25$, in better agreement with the AA model, $p(\text{H}) = 0.36$. Both CG models sample the E region with comparable accuracy. The minimal CG representation (i.e., mapping and interaction set) prevents a quantitative reproduction of the AA cross-correlations, such that both CG-sb and a corresponding force-matching model demonstrate difficulties in stabilizing helices [36]. This deficiency was linked to the stabilization of spurious intermediates in both models. Critically, the CG* model samples fewer of these intermediates ($\Psi \approx 70$ deg, $R_{1\text{–}4} \approx 0.95$ nm), compared with CG-sb. We find that models with lower JSD($\hat{\boldsymbol{e}}_1$ || $\hat{\boldsymbol{e}}_1^{\text{BMSM}}$) more significantly prohibit this region. Figure 7 (b) presents the one-dimensional distribution functions along Ψ and $R_{1\text{–}4}$. The CG-sb model provides an improved description of the one-dimensional distributions, in comparison to the force-matching model, by sharpening the minima of the CG potentials [36]. Over-

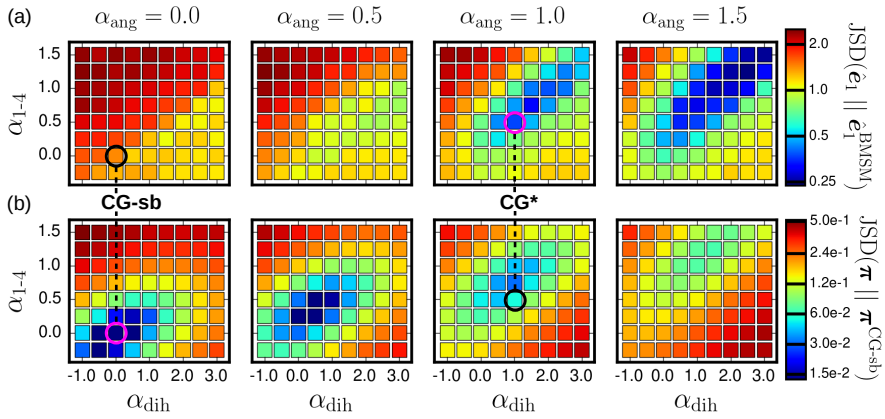

FIG. 6. Ala_4: Assessment of the reparametrized models, each characterized by the scaling parameter $\boldsymbol{\alpha} = \{\alpha_{\rm ang}, \alpha_{\rm dih}, \alpha_{1\text{–}4}\}$ (See Figure 5). (a) Kinetic discrepancies are characterized with respect to the biased MSM (BMSM)—representing the minimal adjustments to the CG-sb model that will yield consistent kinetics—by the Jensen-Shannon divergence (JSD) of the first dynamical eigenvector: $\mathrm{JSD}(\hat{e}_1 \,||\, \hat{e}_1^{\rm BMSM})$. (b) Structural discrepancies are characterized with respect to the original CG-sb model—parametrized with a structure-based scheme—by the JSD of the stationary distribution, $\boldsymbol{\pi}$: $\mathrm{JSD}(\boldsymbol{\pi} \,||\, \boldsymbol{\pi}^{\rm CG\text{-}sb})$). Note that the global minimum of $\mathrm{JSD}(\boldsymbol{\pi} \,||\, \boldsymbol{\pi}^{\rm CG\text{-}sb})$, $\boldsymbol{\alpha} = \{0, 0, 0\}$, falls below the plotted scale ($\approx 10^{-4}$) and is not exactly equal to zero due to small uncertainties in the construction of the MSM.

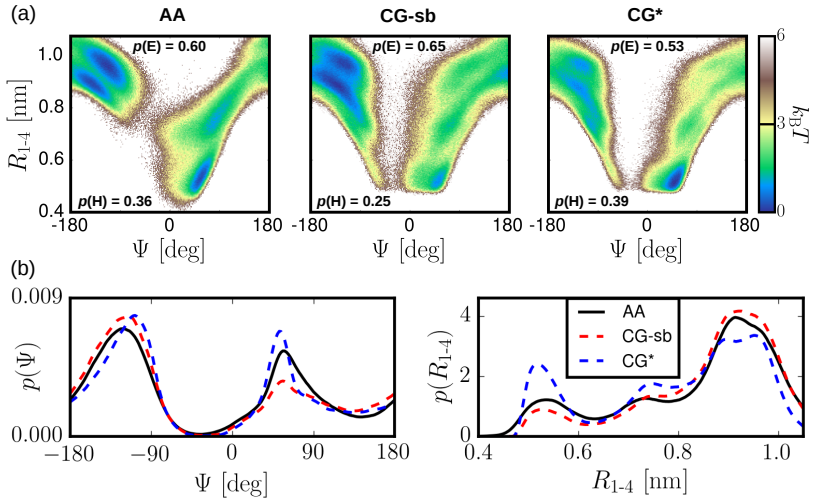

FIG. 7. Ala_4: Structural characterization of the CG* model with respect to the original CG-sb model as well as the reference AA model. (a) Free-energy surfaces along Ψ and $R_{1\text{–}4}$. Probability of sampling the H and E metastable states (see Figure 1) is quantified in each panel. (b) One-dimensional distribution functions along Ψ and $R_{1\text{–}4}$.

all, the CG* model emphasizes the helical region, but retains a qualitative description of the distributions, as compared to CG-sb.

To better monitor the impact of the intermediate region on the nature of the helix-coil transition, we project the free-energy surface along a single parameter, Q, defined orthogonal to the dividing surface between metastable states (Figure 8). The black curve demonstrates that the H to E transition in the AA model occurs via a wide and shallow landscape in the H region, with a narrow but steep dividing surface ($Q \approx 0.3$). Interestingly, the force-matching model constructed by Rudzinski and Noid [36] (CG-fm, cyan curve) reproduces the free-energy along Q rather well, although the lack of a clear minimum in the H region causes serious discrepancies in the one-dimensional distributions and free-energy surface along Ψ and $R_{1\text{–}4}$. In contrast, the CG-sb model (red curve) stabilizes helices via a shallow but narrow minimum in a sub-region of H ($Q \approx -1.0$). Clearly, this shallow minimum along with the lack of a significant barrier between the states causes exceedingly fast H to E transitions, compared with the reverse process [35]. Relative to the CG-sb model, the CG* model (blue curve) significantly stabilizes the narrow helical minimum, while

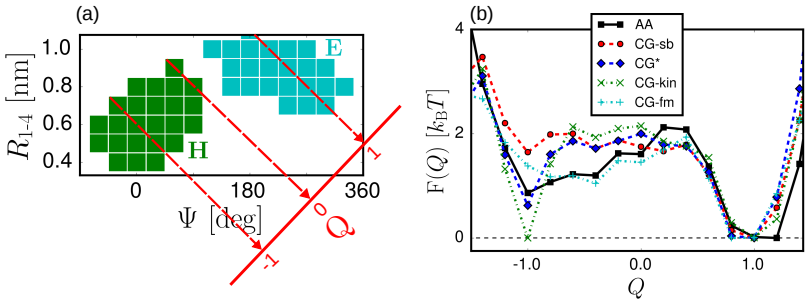

FIG. 8. Ala_4: Projection of the helix-coil transition in Ala_4 onto a single order parameter, Q. (a) Schematic of the projection of the metastable states onto Q. (b) Free-energy profile along Q for the AA model (black curve) and various CG models.

leaving the remainder of the free-energy profile largely unchanged. Consequently, the effective barrier between H and E regions is much higher. Models that emphasize kinetic over structural accuracy exaggerate this stabilization, e.g., CG-kin, $\boldsymbol{\alpha} = \{1.5, 1.0, 1.0\}$, green curve of Figure 8. In agreement with the biased MSM results, improved kinetics of the CG model require a sharp and deep minimum in the helical region.

Finally, Figure 9 characterizes the kinetic properties of the CG-sb and CG* models with respect to the biased MSM and reference AA models. Figure 9 (a) presents an intensity plot of the eigenvector corresponding to λ_1, which characterizes the probability flux at the corresponding timescale. The CG-sb model describes the process quite well, albeit with a slight narrowing of the flux in a small region of the H state [35]. The CG* model demonstrates a similar, but slightly exaggerated, behavior in its eigenvector—a predicted characteristic for consistent kinetics [35]. Figure 9 (b) shows an improved timescale separation between the first and second kinetic processes in the CG* model compared with the CG-sb model. To further assess the description of the slowest process, Figure 9 (c) presents the ratio of mean-first-passage times between the two metastable states. The biased MSM reproduces the AA ratio by construction, while the CG-sb yields an H to E transition which is too fast by about 35%, compared with the reverse process. The CG* model displays significant improvement, nearly quantitatively reproducing this ratio.

IV. CONCLUSIONS

The vast majority of coarse-grained (CG) models display grossly inaccurate kinetic properties—not only is the dynamics overall faster, the slow kinetic processes display inconsistent speedups. Systems as simple as small polypeptides serve as excellent examples: from incompatible forward- and backward-rates (e.g., Ala_4 above) to a swapped hierarchy of the slowest kinetic processes (e.g., Ala_3 above). Rather than a rigorous evolution of CG dynamics, we explore to what extent adjustments of the force field, coupled to a simple Langevin thermostat, can alleviate the issues brought forward by a Markov state model analysis of the statics and kinetics. In particular, the use of *biased* Markov state models, a simulation trajectory augmented with coarse reference information, provides us with two key advantages: (*i*) the use of experimental kinetic information can bypass the requirement to rely on expensive and potentially inaccurate AA simulations; and (*ii*) biased Markov state models can hint at a reparametrization strategy by highlighting the CG potentials' deficiencies.

We find that tuning the difference between CG bead masses can improve the relative timescales of the slow kinetic processes, but does not improve the description of the associated eigenvectors and fails to correct the *order* of kinetic processes. Adjusting the side-chain's bead size of the transferable CG PLUM model can significantly improve the description of the low-populated left-handed helix region in Ala_3, as seen from the relative stability of the different metastable states (i.e., α, β, and α_L). Importantly, we find that the force-field parametrization is still capable of folding the three-helix bundle α3D at a folding temperature in agreement with the original parametrization [39]. The system was too small to probe and possibly refine the interactions modeling hydrogen bonds and hydrophobicity.

Force-field refinement of the structure-based Ala_4 CG model proved most insightful. The original parametrization, aimed to reproduce one-dimensional correlation functions [36], lacked stabilization of the helical state, partially due to spurious intermediates forbidden at the AA level. Here, we find that alternative force-field parameters targeting both static and kinetic properties can retain the overall quality of the one-dimensional distribution functions, while improving the consistency of transitions between metastable states. More specifically, kinetic constraints can restrict the stability of the connecting intermediates, yielding an improved description of transitions.

Although CG potentials that generate a particular set of one-dimensional distributions are unique in theory [63–65], the force field parameters are often highly degenerate in practice [66–68] (i.e., many distinct potentials may

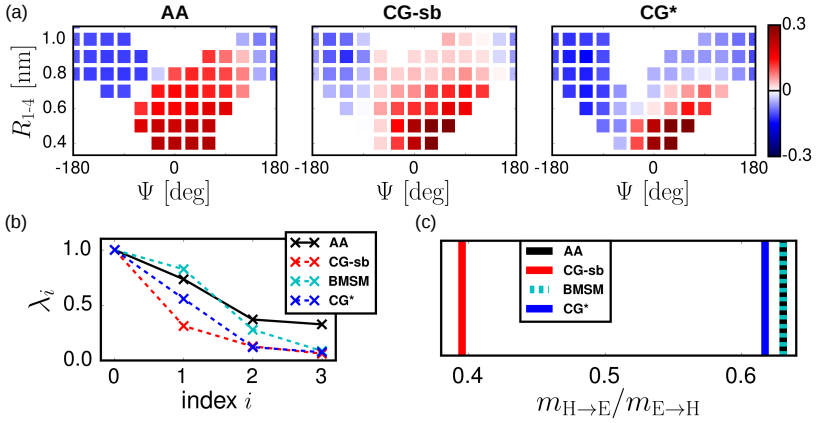

FIG. 9. Ala_4: Kinetic characterization of the CG* model, compared with the CG-sb model, with respect to the biased MSM (BMSM) and reference AA models. (a) Intensity plots of the first dynamical eigenvectors, characterizing the probability flux of each microstate at the corresponding timescale. (b) Eigenvalue spectrum of the three slowest processes. (c) Ratio of mean-first-passage times between the H and E metastable states.

give rise to *nearly* identical distributions). Thus, similar to previous approaches that couple structure-based schemes with additional (e.g., thermodynamic [69, 70]) constraints, consideration of kinetic information can assist in building more robust CG models. Additionally, matching low order distribution functions alone often explicitly deteriorates the description of cross-correlations [54], which may be generally important for accurately modeling the hierarchical structures stabilized by many biological molecules (e.g., proteins). Consequently, we expect force-field parametrization strategies that combine static and kinetic properties to be of use to simulators, even when probing static properties alone.

V. ACKNOWLEDGEMENTS

We thank Anton Melnyk and Svenja Wörner for critical reading of the manuscript. We are also very grateful to Will Noid for the use of the Ala_4 CG models and simulation trajectories. Funding from the SFB-TRR146 grant (JFR) and an Emmy Noether fellowship (TB) of the German Research Foundation (DFG), as well as a Humboldt Fellowship (JFR) from the Alexander von Humboldt Foundation are gratefully acknowledged. We dedicate this work to Kurt Kremer, on the occasion of his 60th birthday, whose guidance, advice, and encouragements foster an enriching scientific experience within the Theory Group of the Max Planck Institute for Polymer Research.

[1] W.F. van Gunsteren, H.J. Berendsen, Angew. Chem. Int. Ed. Engl. **29**, 992 (1990)
[2] M. Karplus, J.A. McCammon, Nat. Struct. Mol. Biol. **9**, 646 (2002).
[3] T.J. Lane, D. Shukla, K.A. Beauchamp, V.S. Pande, Curr. Opin. Struct. Biol. **23**, 58 (2013)
[4] C. Neale, W.D. Bennett, D.P. Tieleman, R. Pomès, J. Chem. Theory Comput. **7**, 4175 (2011)
[5] W. Tschöp, K. Kremer, J. Batoulis, T. Bürger, O. Hahn, Acta Poly. **49**, 61 (1998).
[6] K. Kremer, F. Müller-Plathe, Mol. Sim. **28**, 729 (2002).
[7] C. Peter, K. Kremer, Soft Matter **5**, 4357 (2009)
[8] G.A. Voth (ed.), *Coarse-Graining of Condensed Phase and Biomolecular Systems* (CRC Press, Boca Raton, FL USA, 2009)
[9] S. Riniker, J.R. Allison, W.F. van Gunsteren, Phys. Chem. Chem. Phys. **14**, 12423 (2012).
[10] W. Noid, J. Chem. Phys. **139**, 090901 (2013)
[11] V.A. Harmandaris, D. Reith, N.F.A. Van der Vegt, K. Kremer, Macromol. Chem. Physic. **208**, 2109 (2007).
[12] V.A. Harmandaris, K. Kremer, Soft Matter **5**, 3920 (2009).
[13] K.M. Salerno, A. Agrawal, D. Perahia, G.S. Grest, Phys. Rev. Lett. **116**, 058302 (2016).
[14] R. Zwanzig, Phys. Rev. **124**, 983 (1961)
[15] H. Mori, Prog. Theor. Phys. **33**, 423 (1965)
[16] S. Izvekov, G.A. Voth, J. Chem. Phys. **125**, 151101 (2006).
[17] C. Hijon, P. Espanol, E. Vanden-Eijnden, R. Delgado-Buscalioni, Faraday Disc. **144**, 301 (2010).

[18] S. Markutsya, M.H. Lamm, J. Chem. Phys. **141**, 174107 (2014).

[19] S. Izvekov, B.M. Rice, J. Chem. Phys. **140** (2014)

[20] G. Deichmann, V. Marcon, N.F.A. van der Vegt, J. Chem. Phys. **141**, 224109 (2014)

[21] A. Davtyan, J.F. Dama, G.A. Voth, H.C. Andersen, J. Chem. Phys. **142**, 154104 (2015)

[22] I. Lyubimov, M. Guenza, J. Chem. Phys. **138**, 12A546 (2013)

[23] N. Guttenberg, J.F. Dama, M.G. Saunders, G.A. Voth, J. Weare, A.R. Dinner, J. Chem. Phys. **138**, 094111 (2013).

[24] J.D. Chodera, W.C. Swope, J.W. Pitera, K.A. Dill, Multiscale Model. Simul. **5**, 1214 (2006).

[25] F. Noé, C. Schütte, E. Vanden-Eijnden, L. Reich, T.R. Weikl, Proc. Natl. Acad. Sci. USA **106**, 19011 (2009).

[26] Bowman, Gregory R. and Pande, Vijay S. and Noé, Frank (eds.), *An Introduction to Markov State Models and Their Application to Long Timescale Molecular Simulation* (Springer Science and Business Media, Dordrecht, Netherlands, 2014)

[27] J.D. Chodera, V.S. Pande, Proc. Natl. Acad. Sci. USA **108**, 12969 (2011).

[28] T.J. Lane, G.R. Bowman, K. Beauchamp, V.A. Voelz, V.S. Pande, J. Am. Chem. Soc. **133**, 18413 (2011).

[29] G.R. Bowman, V.A. Voelz, V.S. Pande, J. Am. Chem. Soc. **133**, 664 (2011).

[30] I. Buch, T. Giorgino, G. De Fabritiis, Proc. Natl. Acad. Sci. USA **108**, 10184 (2011).

[31] G.R. Bowman, P.L. Geissler, Proc. Natl. Acad. Sci. USA **109**, 11681 (2012).

[32] N. Plattner, F. Noé, Nat. Commun. **6**, 7653 (2015).

[33] D. Shukla, A. Peck, V.S. Pande, Nat. Commun. **7**, 10910 (2016)

[34] W. Humphrey, A. Dalke, K. Schulten, J. Mol. Graphics **14**, 33 (1996)

[35] J.F. Rudzinski, K. Kremer, T. Bereau, J. Chem. Phys. **144**, 051102 (2016)

[36] J.F. Rudzinski, W.G. Noid, J. Chem. Theor. Comp. **11**, 1278 (2015).

[37] W.L. Jorgensen, D.S. Maxwell, J. Tirado-Rives, J. Am. Chem. Soc. **118**, 11225 (1996).

[38] H. Berendsen, J. Grigera, T. Straatsma, J. Phys. Chem. **91**, 6269 (1987).

[39] T. Bereau, M. Deserno, J. Chem. Phys. **130**, 235106 (2009)

[40] G.T. Ramachandran, V. Sasisekharan, Adv. Protein Chem. **23**, 283 (1968)

[41] T. Bereau, M. Bachmann, M. Deserno, J. Am. Chem. Soc. **132**, 13129 (2010)

[42] T. Bereau, M. Deserno, M. Bachmann, Biophys. J. **100**, 2764 (2011)

[43] T. Bereau, M. Deserno, J. Membrane Biol. **248**, 395 (2014)

[44] T. Bereau, W.D. Bennett, J. Pfaendtner, M. Deserno, M. Karttunen, J. Chem. Phys. **143**, 243127 (2015)

[45] T. Bereau, C. Globisch, M. Deserno, C. Peter, J. Chem. Theory Comput. **8**, 3750 (2012)

[46] K. Osborne, M. Bachmann, B. Strodel, in *From Computational Biophysics to Systems Biology (CBSB11) 2012*, (Proceedings, 20-22 July 2011, Julich, Germany), p. 151

[47] K.L. Osborne, M. Bachmann, B. Strodel, Proteins: Struct., Funct., Bioinf. **81**, 1141 (2013)

[48] K.L. Osborne, B. Barz, M. Bachmann, B. Strodel, Phys. Proc. **53**, 90 (2014)

[49] G.O. Rutter, A.H. Brown, D. Quigley, T.R. Walsh, M.P. Allen, Phys. Chem. Chem. Phys. **17**, 31741 (2015)

[50] Z.J. Wang, M. Deserno, J. Phys. Chem. B **114**, 11207 (2010)

[51] T. Bereau, Z.J. Wang, M. Deserno, J. Chem. Phys. **140**, 115101 (2014)

[52] H.J. Limbach, A. Arnold, B.A. Mann, C. Holm, Comput. Phys. Comm. **174**, 704 (2006)

[53] H.M. Cho, J.W. Chu, J. Chem. Phys. **131**, 134107 (2009).

[54] J.F. Rudzinski, W.G. Noid, J. Phys. Chem. B **118**, 8295 (2014).

[55] J.H. Prinz, H. Wu, M. Sarich, B. Keller, M. Senne, M. Held, J.D. Chodera, C. Schütte, F. Noé, J. Chem. Phys. **134**, 174105 (2011).

[56] G.R. Bowman, K.A. Beauchamp, G. Boxer, V.S. Pande, J. Chem. Phys. **131**, 124101 (2009).

[57] F. Noé, coworkers. Pyemma. `https://github.com/markovmodel/PyEMMA/` (2015)

[58] M. Senne, B. Trendelkamp-Schroer, A.S.J.S. Mey, C. Schütte, F. Noé, J. Chem. Theor. Comp. **8**, 2223 (2012).

[59] M.K. Scherer, B. Trendelkamp-Schroer, F. Paul, G. Pérez-Hernández, M. Hoffmann, N. Plattner, C. Wehmeyer, J.H. Prinz, F. Noé J. Chem. Theor. Comp. **11**, 5525 (2015)

[60] S. Kullback, R.A. Leibler, Ann. Math. Stat. **22**, 79 (1951).

[61] T. Bereau, *Unconstrained structure formation in coarse-grained protein simulations.* Ph.D. thesis, Carnegie Mellon University (2011)

[62] S.T. Walsh, H. Cheng, J.W. Bryson, H. Roder, W.F. DeGrado, Proc. Natl. Acad. Sci. USA **96**, 5486 (1999)

[63] R.L. Henderson, Phys. Lett. A **49**, 197 (1974).

[64] J.T. Chayes, L. Chayes, E.H. Lieb, Comm. Math. Phys. **93**, 57 (1984).

[65] J.F. Rudzinski, W.G. Noid, J. Chem. Phys. **135**, 214101 (2011).

[66] H.C. Andersen, D. Chandler, J.D. Weeks, Adv. Chem. Phys. **34**, 105 (1976).

[67] F. Müller-Plathe, ChemPhysChem **3**, 754 (2002).

[68] J.F. Rudzinski, W.G. Noid, J. Phys. Chem. B **116**, 8621 (2012).

[69] P. Ganguly, D. Mukherji, C. Junghans, N.F.A. van der Vegt, J. Chem. Theor. Comp. **8**, 1802 (2012).

[70] N.J.H. Dunn, W.G. Noid, J. Chem. Phys. **143** (2015).